Chemical Engineering Journal 146 (2009) 105–111

Contents lists available at ScienceDirect

Chemical Engineering Journal

journal homepage: www.elsevier.com/locate/cej

Silicon-based micro-reactor for preferential CO oxidation

Sun-Mi Hwang [a], Oh Joong Kwon [b], Sang Hyun Ahn [a], Jae Jeong Kim [a,*]

[a] Research Center for Energy Conversion and Storage, School of Chemical and Biological Engineering, Seoul National University, San 56-1, Shillim-dong, Kwanak-gu, Seoul, 151-742, Republic of Korea
[b] Department of Mechanical Engineering, University of Incheon, 177, Dohwa-dong, Nam-gu, Incheon, 402-749, Republic of Korea

ARTICLE INFO

Article history:
Received 24 April 2008
Received in revised form 21 August 2008
Accepted 29 August 2008

Keywords:
Micro-reactor
Preferential CO oxidation
Selective CO oxidation
Catalyst coating
Micro-channel
Channel design

ABSTRACT

A silicon-based micro-reactor was fabricated using a micro-electromechanical system (MEMS) process and silicon micromachining technology (SMT) to allow preferential CO oxidation (PrOx) to be applied to compact portable devices. To design the micro-PrOx reactor, the effects of channel length, channel width, channel array, and O_2 content in the reactant gas on the CO conversion and selectivity for CO were investigated. The single micro-PrOx reactor required an O_2 concentration four times higher than the theoretical quantity for a complete conversion of 1% CO into CO_2. The optimum operating temperature to obtain high CO conversion, by suppressing the reverse water–gas shift (r-WGS) reaction, depended considerably on the channel lengths of the micro-reactor rather than on the channel widths or the channel arrays. The micro-PrOx reactor showed 99.4% conversion of CO and 44.14% selectivity for CO at 260 °C when operating with 1% CO, 50% H_2, 35% CO_2, N_2 (balance), and 2% O_2.

1. Introduction

In recent years, the proton exchange membrane fuel cell (PEMFC) has received increased attention owing to its characteristics of being an eco-friendly and efficient energy source for stationary as well as portable applications. In particular, the PEMFC has been considered as a power generator for compact devices such as notebook computers, cellular phones and MP3 players due to its advantages: easy scale-down, fast startup and shutdown, high power density and mild operating temperature (about 60–70 °C). Although the most desirable fuel for a PEMFC is pure H_2, an alternative fuel is required to overcome problems such as storage, safety and refueling of H_2 when the PEMFC is adopted as an energy source for portable devices [1–3]. One substitute for pure H_2 is a reforming system using hydrocarbons such as methanol, ethanol, methane or gasoline. H_2-rich reformed gas produced through steam reforming (SR) and water–gas shift (WGS) reactions generally contains about 0.5–1 vol.% CO [1–4]. The amount of CO must be reduced below 10 ppm because Pt-based anode catalyst of a PEMFC is easily poisoned by a trace amount of CO at low operating temperatures, resulting in the degradation of the PEMFC performance [5]. There are several methods to reduce the CO concentration, such as palladium-based membrane purification, catalytic CO methanation, adsorption purification and preferential CO oxidation (PrOx). Palladium-based membrane purification needs high pressure and temperature, adsorption purification demands a vast volume for adsorbents, and CO methanation (Eq. (3)) consumes large amounts of H_2, compared with preferential CO oxidation (Eq. (1)). Therefore, the most effective way to eliminate CO is by preferential oxidation because of the low process cost, moderate operating temperature and atmospheric pressure operation [6–8].

- Preferential CO oxidation [9]

$$CO + 0.5O_2 \rightarrow CO_2 \quad \Delta H_{298} = -283.0\,kJ\,mol^{-1} \quad [desiredreaction] \tag{1}$$

$$H_2 + 0.5O_2 \rightarrow H_2O \quad \Delta H_{298} = -242.0\,kJ\,mol^{-1} \quad [undesiredreaction] \tag{2}$$

- Methanation [10]

$$CO + 3H_2 \rightarrow CH_4 + H_2O \quad \Delta H_{298} = -283.6\,kJ\,mol^{-1} \tag{3}$$

- Water–gas shift [9,10]

$$CO + H_2O \rightarrow CO_2 + H_2 \quad \Delta H_{298} = -41.1\,kJ\,mol^{-1} \tag{4}$$

In PrOx, the desired reaction is the oxidation of CO by O_2 in H_2-rich reformed gas (Eq. (1)). However, the main product in the reformed gas (H_2) is competitively oxidized by O_2 as in Eq. (2). Thus, it is important to minimize the oxidation of H_2 to improve the efficiency of the PrOx reaction. Pt/Al_2O_3 has been the most suitable catalyst because of its high activity for CO oxidation and

* Corresponding author. Tel.: +82 2 880 8863; fax: +82 2 888 7295.
E-mail address: jjkimm@snu.ac.kr (J.J. Kim).

1385-8947/$ – see front matter © 2008 Elsevier B.V. All rights reserved.
doi:10.1016/j.cej.2008.08.037

its stability at relatively low temperatures [11]. Nevertheless, many researchers have focused on various catalyst systems, not only to increase catalytic activity, selectivity and stability, but also to minimize H_2 oxidation (Eq. (2)). One solution is to use Pt-based catalysts with catalytic characteristics that have been modified by alloying with metals such as Fe [12], Ce [13], Ni, or Co [14]. Other studies have observed the effect of support materials (Al_2O_3, CeO_2, MnO_x, or α-Fe_2O_3) [4,15,16], particle size by a water pretreatment method [17] and other supported metals (Au [18], Rh, Ru, or Pd [19,20]) on the PrOx performance.

Because the two reactions that occur in a PrOx reactor are exothermic (Eqs. (1) and (2)), heat management, i.e. easy removal of the heat generated, in a PrOx reactor is important. Large scale packed-bed reactors have problems such as hot spots, delays in startup or shutdown and mass and heat transfer limitations. Srinivas et al. [21] compared micro-reactors using thin film catalysts with packed-bed reactors using powder or pellet type catalysts for the PrOx reaction. They found that the pressure drop of packed-bed reactors is 400 times higher than that associated with wall coated micro-channels when the two reactors have same catalyst loading and cross-section. Micro-reactors with thin film catalysts have negligible external and internal mass-transport limitations and enhanced heat-transport characteristics compared to packed-bed reactors. This more efficient removal of heat results in their being no large temperature gradient across the catalyst bed and no hot spots in the case of micro-reactors [11]. The advantages of micro-reactors include fast heating and cooling, suppression of hot spots, large surface-area-to-volume ratios, higher conversion and selectivity, fast response and easy integration with miniaturized chemical devices, sensors, actuators, fuel processors, heat exchangers, fuel cells, medical devices, etc. Delsman et al. [22] described that temperature disequilibrium, caused by exothermic reaction of PrOx, of micro-device for PrOx could be minimized by integration with a micro heat exchanger. Kwon et al. [23,24] described a miniaturized reformer–PrOx–fuel cell system based on silicon fabrication technology, and silicon-based PEMFC was successfully operated using hydrogen from methanol reformer and PrOx. Shin et al. [25] investigated a micro-fuel processor (steam reformer and PrOx) using low temperature co-fired ceramic (LTCC), Tanaka et al. [26] demonstrated a miniature fuel cell with a fuel reformer system by micro-electromechanical system (MEMS) technology, and Holladay et al. [27] showed a way to improve thermal efficiency of a micro-scale methanol processor.

In this study, the effects of the design of micro-channels on the performance of a silicon-based micro-PrOx reactor were examined as a function of channel length, channel width and the arrangement of channel arrays, which is related to gas hourly space velocity (GHSV). The design of micro-channel is important to get the optimum performance from the micro-reactor, however, the design of channel has not been much considered in micro-reactor besides manifold geometry of micro-reactor for uniform flow distribution [28].

2. Fabrication

A parallel multi-channeled micro-reactor for PrOx reaction was fabricated on 500 μm thick p-type (1 1 0) silicon wafer by silicon micromachining technology (SMT) designed for MEMS applications. A schematic diagram of the fabrication process is described in Fig. 1. Various reactor patterns were transferred by photolithography onto the (1 1 0) silicon wafer (Fig. 1(a)). To obtain rectangular micro-channels, the silicon wafer was anisotropically etched with 30 wt.% KOH solution at 80 °C for 2 h (Fig. 1(b)) [29]. The etched silicon wafer was assembled with a thin Pyrex™ glass plate by anodic bonding to form a compact and airtight device. The inlet and outlet holes were fabricated on the top of the Pyrex™ glass to make the reactant gas easily accessible (Fig. 1(c)) [23,24]. The micro-PrOx reactor had 17 parallel channels, each with 600 μm width, 240 μm depth and 2.3 cm length as shown in Fig. 2(a) and (b). Micro-reactors with various channel lengths from 2.3 to 13.6 cm and widths from 200 to 600 μm were also designed to examine the effect of channel length and width on the performance of the micro-PrOx reactor.

Prior to catalyst coating, a SiO_2 layer (about 24–27 Å thick) was formed on the inner walls of the micro-channels, by heat treatment at 300 °C for 3 h [30], to act as an adhesive layer between the silicon surface and catalyst layer. The micro-channels were coated with Pt/Al_2O_3 catalyst slurry in accordance with a fill-and-dry coating method [31]. Micro-channels covered with the SiO_2 adhesive layer were filled with the Pt/Al_2O_3 catalyst slurry and the reactor was dried at room temperature and calcined at 500 °C to form a thick catalyst layer only on the inner walls of the micro-channels (Fig. 1(d) and Fig. 3).

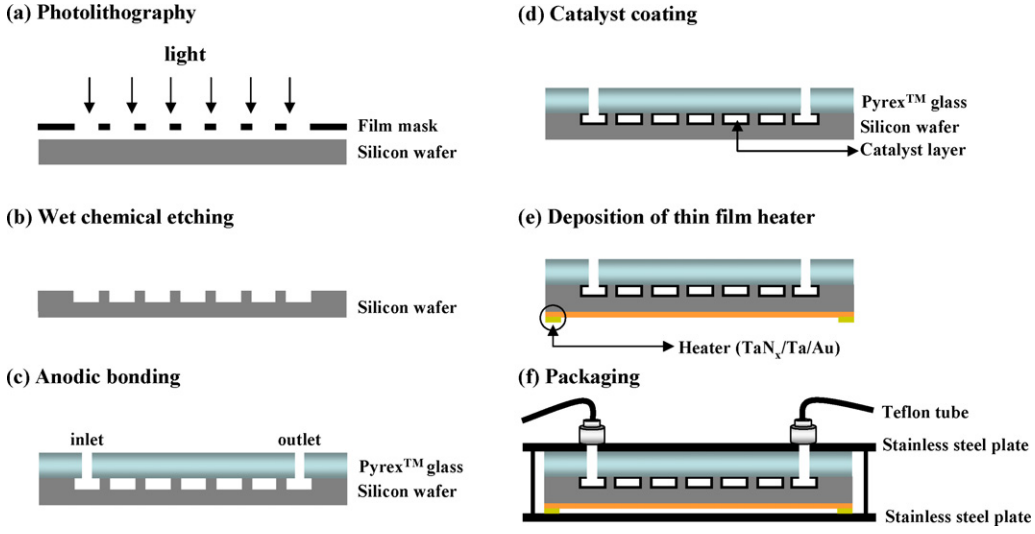

Fig. 1. Fabrication sequences of micro-PrOx reactor.

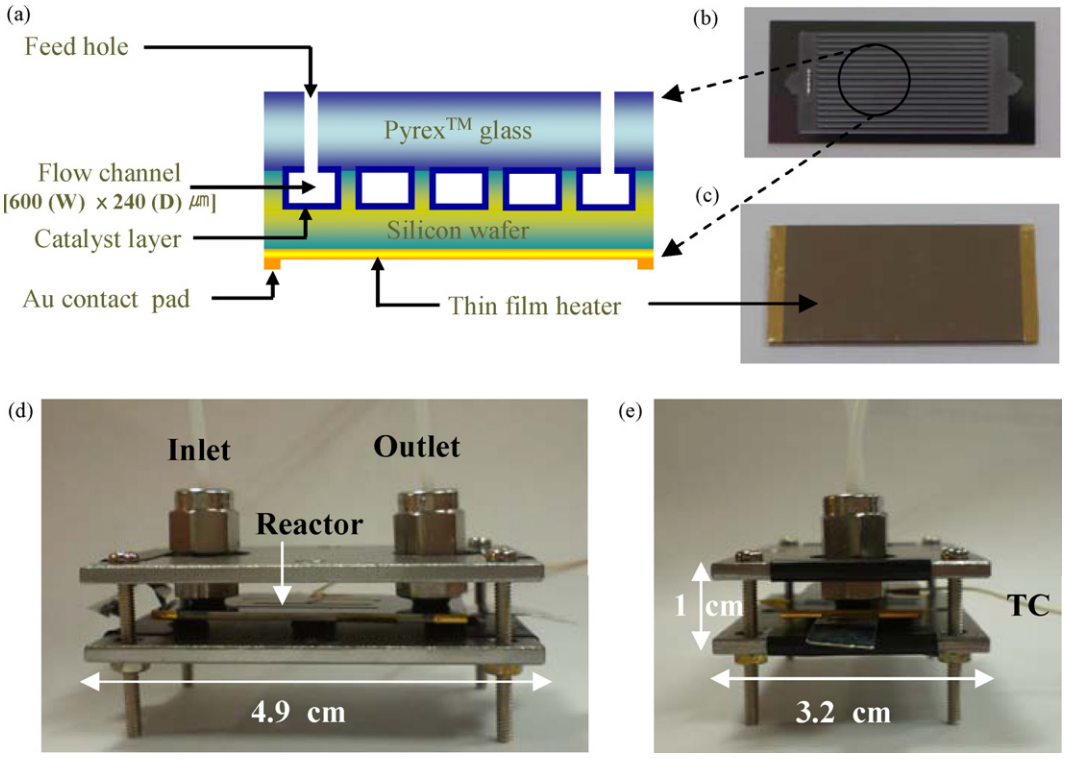

Fig. 2. (a) Schematic diagram of micro-reactor; (b) single micro-reactor; (c) thin film heater on the back side of micro-reactor; (d) front view; and (e) side view of micro-PrOx reactor after packaging.

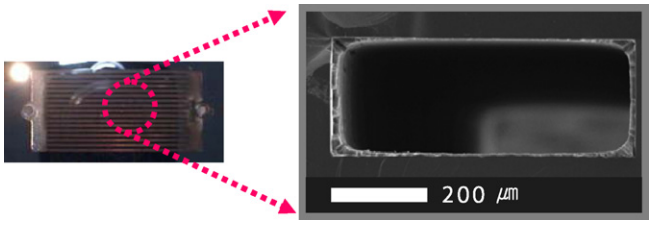

Fig. 3. Cross-sectional SEM image of micro-channel coated with 5 wt.% Pt/Al_2O_3 catalyst slurry by a fill-and-dry coating method.

Following the catalyst coating, a thin film heater was deposited on the back side of the silicon wafer by direct current magnetron sputtering to control the precise temperature of the micro-PrOx reactor. A thin film (80 nm) of TaN_x compound was used as heating material, and a thin Ta layer (a few nm) was deposited on the TaN_x film as an adhesion layer between the TaN_x and an Au contact pad. The Au contact pad (300 nm) was introduced to reduce the contact resistance of TaN_x when external electric power was supplied (Fig. 1(e) and Fig. 2(c)). The temperature of the thin film heater was controlled by a temperature controller that included a power supply, a relay and a proportional integral differential (PID) program [23,24,30]. The fabricated micro-PrOx reactor was packaged with a stainless steel end-plate to test the activity, as displayed in Fig. 1(f), and Fig. 2(d) and (e). The volumes of the micro-PrOx reactor before and after packing were 0.666 and 15.68 cm^3, respectively.

3. Experimental

In this study, a commercial 5 wt.% Pt/Al_2O_3 (Johnson Matthey) catalyst was used for preferential CO oxidation in all experiments. The catalyst slurry used to coat the inner walls of the micro-channels was composed of a mixture of alumina sol, distilled (DI) water, and catalyst (alumina sol:DI water:catalyst = 1:8:1) prepared by ball milling for 5 days. Viscosity of the catalyst slurry after ball milling was measured by rheometer (Bohlin Instrument). After coating with the catalyst, the cross-sectional morphology and thickness of the catalyst layer were examined by a field emission scanning electron microscope (FESEM).

To measure the activity of the preferential CO oxidation, a standard gas mixture composed of 1% CO, 50% H_2, 35% CO_2 and balance N_2 was adopted. 1–2% O_2 (λ = 2–4) was added for oxidation of CO (here, lambda (λ) refers to the oxygen excess factor, which is defined as the ratio of the concentration of O_2 to the concentration of CO ($\lambda = 2[O_2]/[CO]$)) [32]. The flow rates of the standard gas mixture were controlled by mass flow controllers (MFC, Bronkhorst); the total gas flow rate was 204 mL min^{-1} in all micro-reactors and the gas hourly space velocity in the range of 36,230–217,390 h^{-1} was varied by the geometry of micro-channel in this experiment.

After the PrOx reaction, the outlet gas composition from the micro-PrOx reactor was analyzed by micro gas chromatography (CP 4900, Varian). Two columns (Molsieve 5A for H_2, CO and O_2 detection, and PoraPLOT Q for CO_2 detection) were used, with thermal conductivity detectors (TCDs) on each. Argon was used as the carrier gas for both columns. The CO detection limit of the micro gas chromatograph was around 5 ppm. The calculated CO conversion was based on the concentrations of CO at the inlet and outlet of the reactor (Eq. (5)). On the assumption that O_2 was only utilized for oxidation of CO and H_2, the selectivity toward CO was defined as the ratio of the amount of O_2 used for CO oxidation to the amount of O_2 consumed in all reactions (Eq. (6)).

$$\text{Conversion of CO (\%)} = \left(\frac{[CO]_{inlet} - [CO]_{outlet}}{[CO]_{inlet}}\right) \times 100 \quad (5)$$

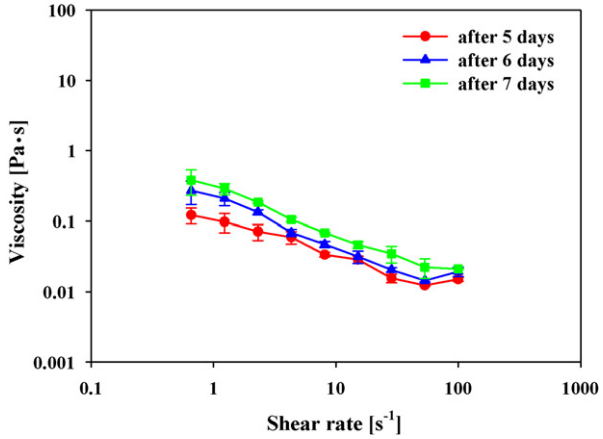

Fig. 4. Viscosity of Pt/Al_2O_3 catalyst slurry at different ball milling time.

$$\text{Selectivity toward CO (\%)} = \left\{\frac{0.5([CO]_{inlet}-[CO]_{outlet})}{[O_2]_{inlet}-[O_2]_{outlet}}\right\}\times 100 = \left\{\frac{[CO]_{inlet}-[CO]_{outlet}}{([CO]_{inlet}-[CO]_{outlet})+([H_2]_{inlet}-[H_2]_{outlet})}\right\}\times 100 \quad (6)$$

4. Results and discussion

The formation of a layer-type catalyst is an important issue in micro-reactor fabrication because the pressure drop in the micro-channels increases and reactant flow is blocked if the micro-channels are packed with catalyst powder or pellets. Thus, a thin film-type catalyst layer was introduced by a fill-and-dry coating method using catalyst slurry. As shown in Fig. 3, a 10–15 μm thick catalyst layer was formed onto the inner walls of the micro-channels. The viscosity of the catalyst slurry was proportional to the ball milling time (Fig. 4). In this study, catalyst slurry prepared by ball milling for 5 days was used in all experiments to produce low viscosity slurries, which resulted in thin catalyst layers, thus minimizing the pressure drop inside of the micro-channels.

The performance of a micro-PrOx reactor coated with Pt/Al_2O_3 catalyst was examined with lambda values of 2 and 4 in the temperature range 190–310 °C at a GHSV of 217,390 h^{-1}. Fig. 5 shows the CO conversion and the selectivity for CO analyzed with a reaction mixture consisting of 1% CO, 50% H_2, 35% CO_2, 1–2% O_2 and N_2 balance. For λ = 2, CO conversion gradually increased from 8.6 to 77.3% with increasing operating temperature up to 290 °C and decreased slightly to 73% above 290 °C. For λ = 4, CO conversion suddenly increased from 35.8 to 99.2% as the operating temperature increased from 230 to 250 °C. A maximum CO conversion of 99.5% was obtained at 260 °C and conversion dropped off slowly as the temperature increased further. The gradual loss of conversion at high temperature after passing maximum conversion is related to the reverse water–gas shift (r-WGS) reaction occurring between CO_2 and H_2, and will be discussed in detail later. For both cases (λ = 2 and 4), the selectivity and conversion of CO showed a similar trend with temperature. Increasing the O_2 concentration resulted in a dramatic increase in the conversion of CO and reduced operating temperature window. Unlike the general trend in the conventional packed-bed PrOx reactor which shows a decrease in CO selectivity with O_2 concentration, the selectivity for CO in the micro-PrOx

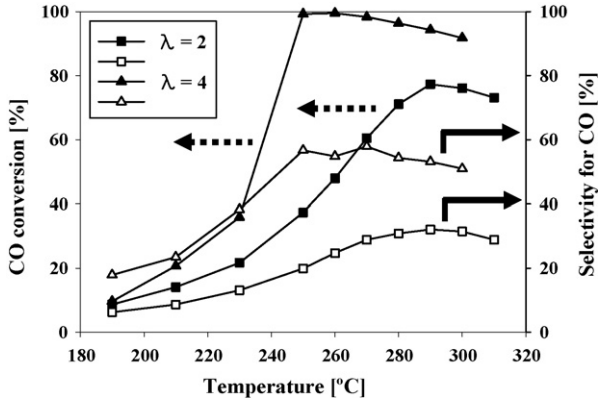

Fig. 5. CO conversion and selectivity vs. reaction temperatures at different lambdas (λ = 2 and 4).

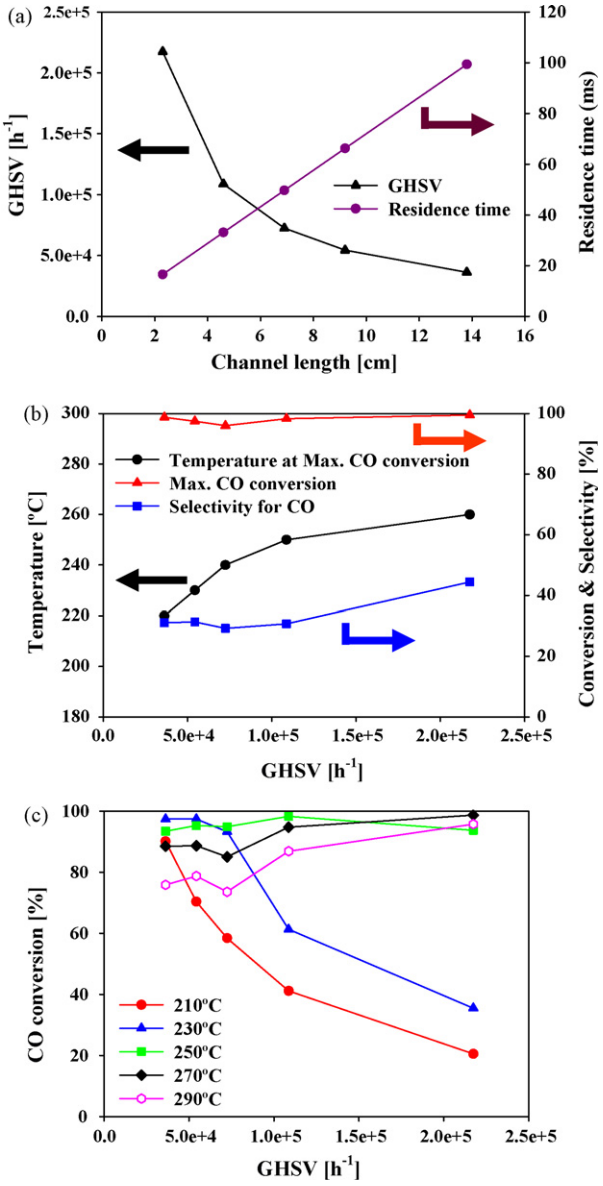

Fig. 6. (a) Relation between channel length and GHSV; (b) conversion, selectivity for CO, and reaction temperatures at maximum CO conversion with increasing GHSV; and (c) CO conversion vs. GHSV value controlled by channel length at particular operating temperatures.

reactor increased in spite of increasing the O_2 concentration. An O_2 concentration at least fourfold higher than the stoichiometric value was required to fully convert CO to CO_2 in the micro-PrOx reactor. Our micro-reactor has relatively higher GHSV than other micro-reactors (a factor of 145) [11] or conventional reactors (a factor of 10) [33]. The higher GHSV causes the reduction of O_2 consumption because much O_2 pass through the system without reaction with adsorbed CO on the catalyst bed. Another possible reason for needing a high O_2 concentration is the lack of insulator for the micro-reactor used in the present experiment. The resulting heat loss may mean that the PrOx reaction occurred incompletely at lower O_2 concentrations. For the reasons mentioned above, a higher O_2 concentration was needed to achieve 100% CO conversion. Thus, all subsequent experiments were conducted at the condition of $\lambda = 4$.

The design of channel length in micro-PrOx reactor affects the performance of the PrOx reaction with the GHSV in the micro-reactor. The GHSV was decreased from 217,390 to 36,230 h^{-1} by increasing the channel lengths of the micro-channels from 2.3 to 13.8 cm, as shown in Fig. 6(a). Fig. 6(b) shows that the temperature of maximum CO conversion decreased monotonically from 260 to 220 °C with decreasing GHSV over the full range of values achieved by variation of channel length. The maximum CO conversion reduced slightly from 99.49 to 95.98% as the GHSV decreased from 217,390 to 72,460 h^{-1}, and then elevated to 98.74% for the GHSV of 36,230 h^{-1}. The highest CO selectivity of 44.4% was obtained with the highest GHSV of 217,390 h^{-1}. However, the selectivity for CO was independent of GHSV for values of GHSV lower than 108,700 h^{-1}. The selectivity stabilized at around 30% after a sharp drop from 44.4 to 30.74% between the GHSV values of 217,390 and 108,700 h^{-1}. Fig. 6(c) shows the effect of variation of GHSV by channel length on the CO conversion at a series of five fixed operating temperatures. Below 250 °C, the CO conversion gradually improved with decreasing GHSV, from 20.55 to 90.13% at 210 °C and from 35.52 to 97.41% at 230 °C. Above 250 °C, however, the CO conversion in the micro-PrOx reactor presented the reverse trend, decreasing significantly from 98.68 to 88.53% at 270 °C, and from 95.74 to 75.88% at 290 °C, with decreasing GHSV. The decline in CO conversion can occur by r-WGS at both higher and lower GHSV, however, it is much more affected by r-WGS at lower GHSV and high operating temperature [33,34]. When the r-WGS reaction is accelerated at higher operating temperatures, it sets a thermodynamic limited to the extent of CO conversion (Eq. (7)) under conditions of abundant of CO_2 and H_2 in the reactant [8,34–36].

- Reverse water–gas shift reaction [35]

$$CO_2 + H_2 \rightarrow CO + H_2O \qquad \Delta H_{298} = +41.2\ \text{kJ mol}^{-1} \tag{7}$$

The reduction of overall CO conversion due to the r-WGS was more strongly affected by operating temperature than GHSV. Nevertheless, to maintain higher CO conversion and inhibit the r-WGS reaction, control of the GHSV through channel length as well as operating temperature must be considered. The optimum operating temperature varied with the GHSV, i.e. 230 °C < $T_{operating}$ < 250 °C for lower GHSV below 108,700 h^{-1}, and $T_{operating}$ > 250 °C for higher GHSV over 108,700 h^{-1}.The higher GHSV was required to obtain nearly 100% CO conversion as the temperature escalated in order to minimizing the effect of r-WGS. Therefore, the operating temperature range for any channel design can be controlled by the relationship between GHSV controlled by channel lengths and operating temperature.

The effect of channel array on the CO conversion was investigated at equal GHSV. Two types of micro-reactors illustrated in Fig. 7(c), had different lengths and numbers of channels, but each had the same GHSV of 217,390 h^{-1}. The channel length of reactor (1) was two times longer than that of reactor (2), while the number of channels of reactor (2) was double that of reactor (1).

The pressure drop (ΔP) in both reactors was calculated. The reaction rate of CO oxidation is a function of the CO and O_2 partial pressure, which is affected by pressure drop [9,11,37]. The pressure drop was computed both by macroscopic analysis, using an engineering Bernoulli equation [38] and by simulation with Fluent™. To evaluate the pressure drop by macroscopic analysis, it was assumed that the reactant gas was an incompressible Newtonian fluid (no density change in the gas mixture between inlet and outlet). The pressure drops calculated from macroscopic analysis and simulation are tabulated in Table 1. As shown in Fig. 7(a) and (b), the CO

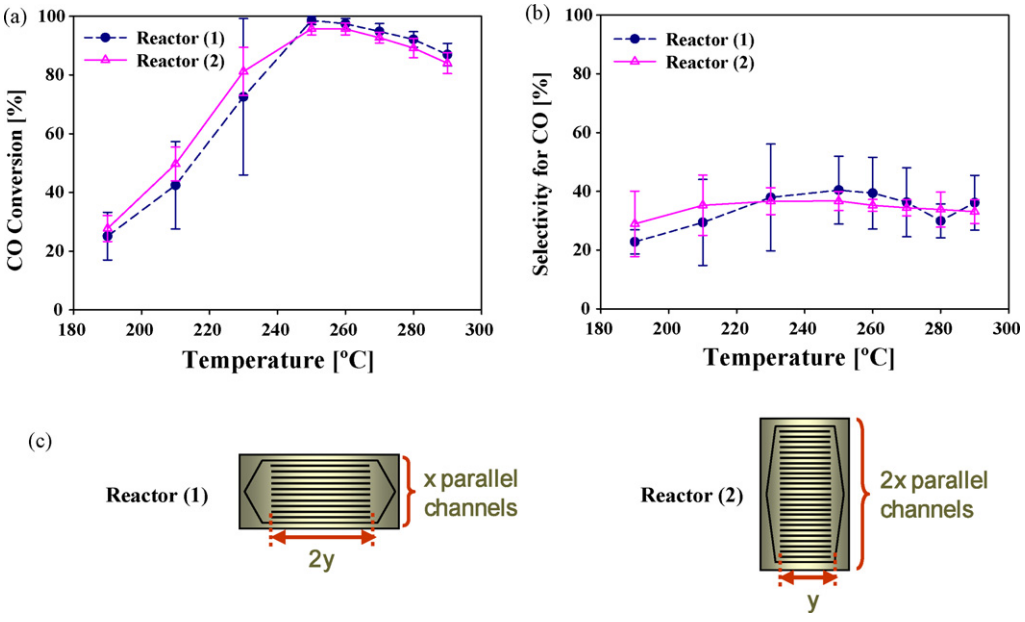

Fig. 7. (a) CO conversion vs. reaction temperatures; (b) selectivity for CO vs. reaction temperatures for reactors (1) and (2); and (c) schematic diagram of two reactors with different channel array geometry.

Table 1
Pressure drop (ΔP) of reactors (1) and (2) in Fig. 7 calculated by macroscopic analysis and Fluent™ simulation

	Reactor (1)	Reactor (2)	(1)/(2)
Simulation by Fluent™	854.04 Pa	410.46 Pa	2.08
Macroscopic analysis	377.55 Pa	391.64 Pa	1.04

Table 2
Pressure drop (ΔP) of reactors (1), (2), and (3) in Fig. 8 calculated by macroscopic analysis and Fluent™ simulation

	Reactor (1)	Reactor (2)	Reactor (3)
Channel width (μm)	600	300	200
Simulation by Fluent™	557.05 Pa	719.19 Pa	1029.02 Pa
Ratio to reactor (1)	–	(2)/(1) = 1.29	(3)/(1) = 1.85
Macroscopic analysis	284.59 Pa	1030.63 Pa	2749.03 Pa
Ratio to reactor (1)	–	(2)/(1) = 3.62	(3)/(1) = 9.66

conversion and selectivity for CO in reactor (1) and (2) did not significantly depend on the channel array because pressure drops in the two micro-reactors were not considerably different for the same GHSV. In reactor (1), as shown in Fig 7(a), the deviation of CO conversion value is bigger than that in reactor (2). It means that the PrOx reaction in reactor (2) becomes more stable than it in reactor (1), which is perhaps because an increase in channel length affects the r-WGS reaction at the outlet of reactor. This is more obvious when the selectivity in reactor (2) is considered. The selectivity for CO in reactor (2) is more stable with temperature, which means that the PrOx reaction in reactor (2) with shorter and many channels is less affected by r-WGS. For the reasons mentioned above, the lower fluctuation of CO conversion in reactor (2) implies that the PrOx reaction takes place more comfortably in reactor (2) than reactor (1).

Fig. 8 exhibits the effect of channel width on CO conversion. To change the width of micro-channels, subchannels were introduced in the parallel channels with 600 μm width and 240 μm depth by inserting inner walls. One inner wall divided a 600 μm wide channel into two 300 μm wide subchannels, and two inner walls made three 200 μm wide subchannels, as illustrated in Fig. 8(c). The total area inside the channels was increased by insertion of an inner wall. The internal surface areas of each channel were 6.57, 8.45 and 10.32 cm^2 for micro-PrOx reactors with 600, 300 and 200 μm wide channels, respectively. The GHSV in all reactors was same with 217,390 h^{-1}. It was expected that the pressure drop in the micro-reactors would be increased by the addition of inner walls and the performance of the micro-PrOx reactor would be affected by the pressure drop. Fig. 8(a) and (b) shows, however, that there is no significant difference in CO conversion in spite of the increase in internal surface area. Table 2 shows the pressure drop at each reactor calculated by simulation using Fluent™ and macroscopic analysis. As I mentioned above, the CO oxidation rate is function of CO and O_2 partial pressure, however, the reaction order with respect of CO partial pressure on Pt/Al_2O_3 is a negative value (around −0.42 to −0.51) [36,37]. This means diminution of the CO oxidation rate with CO partial pressure. The CO coverage on the active surface in the low temperature region becomes almost saturated, while the dissociative adsorption of O_2 on the Pt surface is very low. In this case, the degree of CO coverage decreases with increasing temperature due to partial desorption of CO, and the free Pt sites can use for dissociative adsorption of O_2 [8,39]. Therefore the rate of surface reaction will be limited by the amount of adsorbed CO even though O_2 accessibility to the active catalyst sites increases with O_2 partial pressure when the total pressure is increased. In this case, the CO conversion is insensitive to total pressure. This argument offers one

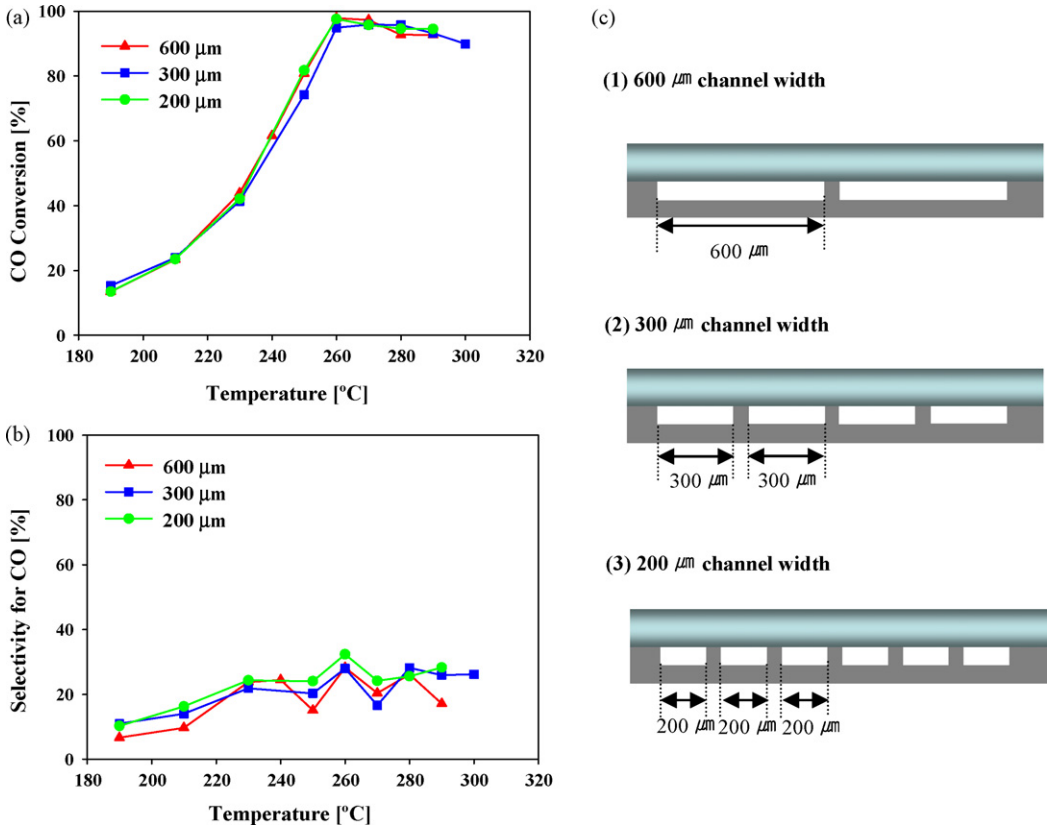

Fig. 8. (a) CO conversion vs. reaction temperatures; (b) selectivity for CO vs. reaction temperatures; and (c) schematic diagram of three reactors with different channel width of 600, 300, and 200 μm.

possible reason for the three reactors in Fig. 8 with different pressure drops, but identical GHSV, showing similar conversion rates.

5. Conclusion

Our research focused on the design aspects of micro-channels, which plays an important role in the determination of the performance of micro-PrOx reactors. To evaluate the effect of the design of the channels, we investigated channel length, channel width and channel array geometry, all of which were related to the GHSV of the reactants. The operation of the micro-PrOx reactor was found to be strongly affected by the channel length. To keep high CO conversion while preventing the r-WGS reaction, the GHSV was increased by reducing the channel length as the temperature increased and the working temperature window and optimum channel length were determined. The CO conversion was not much affected by channel array or width while the GHSV was constant, however, the reaction stability in the micro-PrOx reactor was improved by using a greater number of shorter channels. In the single micro-PrOx reactor, an O_2 concentration at least four times larger than the stoichiometric quantity was needed to get nearly 100% conversion of CO. The optimized micro-PrOx reactor showed 99.4% CO conversion and 44.14% selectivity, using a gas mixture composed of 1% CO, 50% H_2, 35% CO_2, balance N_2 and 2% O_2 with $\lambda = 4$ and temperature at 260 °C.

Acknowledgments

This work was supported by the Korea Science and Engineering Foundation (KOSEF) through the Research Center for Energy Conversion and Storage (RCECS), Inter-University Semiconductor Research Center (ISRC), and Seoul Renewable Energy Research Consortium (Seoul R & BD Program).

References

[1] T. Utaka, T. Takeguchi, R. Kikuchi, K. Eguchi, Appl. Catal., A Gen. 246 (2003) 117–124.
[2] J. Agrell, H. Birgersson, M. Boutonnet, J. Power Sources 106 (2002) 249–257.
[3] Y. Choi, H.G. Stenger, Appl. Catal., B Environ. 38 (2002) 259–269.
[4] F. Mariño, C. Descorme, D. Duprez, Appl. Catal., B Environ. 58 (2005) 175–183.
[5] J.Y. Kim, O.J. Kwon, S.-M. Hwang, M.S. Kang, J.J. Kim, J. Power Sources 161 (2006) 432–436.
[6] M. Kotobuki, A. Watanabe, H. Uchida, H. Yamashita, M. Watanabe, J. Catal. 236 (2005) 262–269.
[7] A. Manasilp, E. Gulari, Appl. Catal., B Environ. 37 (2002) 17–25.
[8] S. Zhou, Z. Yuan, S. Wang, Int. J. Hydrogen Energy 31 (2006) 924–933.
[9] Y. Choi, H.G. Stenger, J. Power Sources 129 (2004) 246–254.
[10] G. Kolb, H. Pennemann, R. Zapf, Catal. Today 110 (2005) 121–131.
[11] X. Ouyang, L. Bednarova, R.S. Besser, AIChE J. 51 (2005) 1758–1772.
[12] A. Sirijaruphan, J.G. Goodwin, R.W. Rice, J. Catal. 224 (2004) 304–313.
[13] I.H. Son, A.M. Lane, Catal. Lett. 76 (2001) 151–154.
[14] E.Y. Ko, E.D. Park, K.W. Seo, H.C. Lee, D. Lee, S. Kim, Catal. Today 116 (2006) 377–383.
[15] R.J.H. Grisel, B.E. Nieuwenhuys, J. Catal. 199 (2001) 48–59.
[16] M.J. Kahlich, H.A. Gasteiger, R.J. Behm, J. Catal. 182 (1999) 430–440.
[17] I.H. Son, A.M. Lane, D.T. Johnson, J. Power Sources 124 (2003) 415–419.
[18] G.K. Bethke, H.H. Kung, Appl. Catal., A Gen. 194–195 (2000) 43–53.
[19] H. Tanaka, S.I. Ito, S. Kameoka, K. Tomishige, K. Kunimori, Catal. Commun. 4 (2003) 1–4.
[20] P.V. Snytnikov, V.A. Sobyanin, V.D. Belyaev, P.G. Tsyrulnikov, N.B. Shitova, D.A. Shlyapin, Appl. Catal., A Gen. 239 (2003) 149–156.
[21] S. Srinivas, A. Dhingra, H. Im, E. Gulari, Appl. Catal., A Gen. 274 (2004) 285–293.
[22] E.R. Delsman, M.H.J.M. De Croon, A. Pierik, G.J. Kramer, P.D. Cobden, Ch. Hofmann, V. Cominos, J.C. Schouten, Chem. Eng. Sci. 59 (2004) 4795–4802.
[23] O.J. Kwon, S.-M. Hwang, J.-G. Ahn, J.J. Kim, J. Power Sources 156 (2006) 253–259.
[24] O.J. Kwon, S.-M. Hwang, J.H. Chae, M.S. Kang, J.J. Kim, J. Power Sources 165 (2007) 342–346.
[25] Y. Shin, O. Kim, J.C. Hong, J.H. Oh, W.J. Kim, S. Haam, C.H. Chung, Int. J. Hydrogen Energy 31 (2006) 1925–1933.
[26] S. Tanaka, K.-S. Chang, K.-B. Min, D. Satoh, K. Yoshida, M. Esashi, Chem. Eng. J. 101 (2004) 143–149.
[27] J.D. Holladay, E.O. Jones, R.A. Dagle, G.G. Xia, C. Cao, Y. Wang, J. Power Sources 131 (2004) 69–72.
[28] G. Griffini, A. Gavriilidis, Chem. Eng. Technol. 30 (2007) 395–406.
[29] H. Hamatsu, M. Nagase, K. Kurihara, K. Iwadate, K. Murase, Microelectron. Eng. 27 (1995) 71–74.
[30] O.J. Kwon, S.-M. Hwang, I.K. Song, H.-I. Lee, J.J. Kim, Chem. Eng. J. 133 (2007) 157–163.
[31] S.-M. Hwang, O.J. Kwon, J.J. Kim, Appl. Catal., A Gen. 316 (2007) 83–89.
[32] A. Wootsch, C. Descorme, D. Duprez, J. Catal. 225 (2004) 259–266.
[33] L. Shore, R.J. Farrauto, in: W. Vielstich, A. Lamm, H.A. Gasteiger (Eds.), Handbook of Fuel Cells-Fundamentals Technology and Applications, vol. 3, John Wiley & Sons, West Sussex, UK, 2003, pp. 211–218.
[34] G.W. Roberts, P. Chin, X. Sun, J.J. Spivey, Appl. Catal., B Environ. 46 (2003) 601–611.
[35] P. Chin, X. Sun, G.W. Roberts, J.J. Spivey, Appl. Catal., A Gen. 302 (2006) 22–31.
[36] D.H. Kim, M.S. Lim, Appl. Catal., A Gen. 224 (2002) 27–38.
[37] M.J. Kahlich, H.A. Gasteiger, R.J. Behm, J. Catal. 171 (1997) 93–105.
[38] M.M. Denn, Process Fluid Mechanics, Prentice-Hall, 1980, pp. 89–91.
[39] A. Sirijaruphan, J.G. Goodwin Jr., R.W. Rice, J. Catal. 227 (2004) 547–551.